

Whole-Genome Transcription Profiling of Rhesus Monkey Rhadinovirus

Dirk P. Dittmer,^{1,2} Carlos M. Gonzalez,^{1,2} Wolfgang Vahrson,¹ Scott M. DeWire,^{2,3}
Rebecca Hines-Boykin,¹ and Blossom Damania^{1,2,3*}

*Department of Microbiology and Immunology,¹ Lineberger Comprehensive Cancer Center,² and
Curriculum in Genetics and Molecular Biology,³ University of North Carolina
at Chapel Hill, Chapel Hill, North Carolina 27599*

Received 11 July 2004/Accepted 21 February 2005

Rhesus monkey rhadinovirus (RRV) and Kaposi's sarcoma-associated herpesvirus (KSHV; also called human herpesvirus 8) belong to the gamma-2 grouping of herpesviruses. RRV and KSHV share a high degree of sequence similarity, and their genomes are organized in a similar fashion. RRV serves as an excellent animal model system to study the gamma herpesvirus life cycle both in vitro and in vivo. We have developed a high-sensitivity, high-throughput, high-specificity real-time quantitative reverse transcriptase-based PCR assay for RRV and have used this assay to profile transcription from the whole RRV genome during de novo productive infection of rhesus fibroblasts. Using this assay, we demonstrate that the genome-wide transcription profile for RRV closely parallels the genome-wide transcription profile for KSHV.

Kaposi's sarcoma (KS)-associated herpesvirus (KSHV; also called human herpesvirus 8) was identified in KS lesions from AIDS patients by using representational differential analysis (6). KS was first described as a cancer of elderly men and is also found in non-human immunodeficiency virus-infected individuals who are immunocompromised, such as transplant recipients. The classic form of KS also occurs in nonimmunocompromised hosts. The KS lesion is comprised of a mixed population of cells including endothelial, inflammatory, and spindle cells. The virus is found in the spindle cells and at times in macrophages in the lesion but not the infiltrating T lymphocytes. KSHV has also been linked to two B-cell lymphoproliferative diseases, namely, primary effusion lymphoma (PEL) and multicentric Castleman's disease (4, 51). In 1997, the New England Primate Research Center reported the isolation of a new herpesvirus, rhesus monkey rhadinovirus (RRV), showing close sequence relatedness to KSHV. Two different RRV isolates were subsequently sequenced at the New England Primate Research Center (RRV strain 26-95) and the Oregon Regional Primate Research Center (RRV strain 17577) (1, 50), and both isolates exhibit high overall sequence similarity to KSHV. The RRV genome, for the most part, is organized in a colinear fashion with KSHV. However, unlike KSHV, RRV grows to high titers in culture and currently represents the closest nonhuman primate model for KSHV and KSHV-associated malignancies.

Wong et al. (57) have reported that naive rhesus macaques that were coinfecting with RRV (strain 17757) and simian immunodeficiency virus developed lymphoid hyperplasia comparable to KSHV-associated multicentric Castleman's disease. Similarly, Mansfield et al. (34) reported that RRV-negative naive macaques infected with RRV (strain 26-95) developed

clinical lymphadenopathy consisting of paracortical and vascular hyperplasia, which over time evolved into marked follicular hyperplasia but ultimately resolved approximately 12 weeks postinfection (34). The phenotypes seen with RRV closely resemble the clinical presentation of KSHV-associated lymphoproliferative diseases and conform to the clinical manifestations of primary gammaherpesvirus infections in the human population. Studying RRV in its natural host overcomes two fundamental roadblocks in KSHV research. First, RRV provides an animal model system to study the relationship between simian immunodeficiency virus and RRV coinfection that can closely model human immunodeficiency virus and KSHV coinfection. Such a model does not otherwise exist for KSHV. Second, studying the lytic life cycle of KSHV is hampered by the fact that at most 20 to 30% of latently infected PEL cells can be reactivated by tetradecanoyl phorbol acetate (TPA) (43). Such TPA reactivation assays are widely used to study KSHV lytic gene expression. Recently, an Rta/ORF50-inducible BCBL-1 cell line was developed to study lytic gene expression (36). Systems to study de novo infection of KSHV, however, are limited by low viral titers and the propensity for KSHV to enter latency after a few passages in tissue culture of infected cells (15, 30, 42, 47). In contrast, RRV can be grown to high titers ($\sim 10^6$ PFU/ml) in primary rhesus fibroblasts (RhFs) and can be serially propagated ad infinitum. This greatly facilitates the construction of recombinant viruses (13) and can be used, for instance, to evaluate loss-of-function phenotypes of mutant viruses after primary infection.

As with other surrogate viruses for human pathogens, the usefulness of the RRV model rests on establishing close correlations between the molecular machinery of RRV and KSHV. We have previously shown that the kinetics of key RRV transcripts after primary infection in RhFs mirror the kinetics of the homologous KSHV transcripts after reactivation in PEL cell lines (12). This can be attributed, in part, to the functional conservation between the major immediate-early transactivator of both viruses, namely, Rta/ORF50. RRV

* Corresponding author. Mailing address: Lineberger Comprehensive Cancer Center, CB #7295, University of North Carolina, Chapel Hill, NC 27599. Phone: (919) 843-6011. Fax: (919) 966-9673. E-mail: damania@med.unc.edu.

open reading frame 50 (ORF50) can transactivate several KSHV promoters, albeit to a lesser extent than KSHV ORF50 (11), and KSHV ORF50 can transactivate a subset of RRV promoters tested to date (12). In order to further elucidate commonalities and differences between RRV and KSHV, we have developed a real-time reverse transcription (RT)-PCR-based array for every mRNA in the entire RRV genome. This assay is high throughput and highly sensitive, making it amenable to profiling of the viral transcription of the more than 80 RRV genes simultaneously and with multiple samples. In this report, we describe the transcription profile of RRV after lytic infection in RhFs.

Real-time QPCR array for RRV. The primary achievement of real-time quantitative PCR (QPCR) is that, for the first time, PCR (and RT-PCR) delivers reliable quantitative information without the need for dilution series or internal competitors, etc. Quantitative information can be extracted because the QPCR is monitored in real time (23) and the reaction product is quantified at every cycle using a double-strand-specific intercalating dye (SYBR). We have recently shown that using the fluorescent dye SYBR is as sensitive as TaqMan-based detection (38) and have thus used SYBR for every primer pair in the RRV QPCR array. This removed one layer of variation, namely, the hybridization efficiency of the indicator oligonucleotide (TaqMan, Beacon, etc.), and yielded a high-throughput, low-cost approach, without compromising sensitivity or linearity (6 orders of magnitude) of the assay.

The RRV primer set is shown in Table 1. Primer design is one of the most important aspects in achieving a successful QPCR array. Based upon our prior experience (16, 19), we used the following guidelines to attain the best primer pairs possible. (i) The melting temperature (T_m) of the primers should be in the range of $59 \pm 2^\circ\text{C}$. The T_m was calculated using the Primer3 program (46) and the default setting for salt (50 mM KCl) and a 50 nM primer DNA concentration. (ii) The maximal difference between two primers within the same primer pair should be no more than 2°C . (iii) The total guanine (G) and cytosine (C) content within any given primer should be 20 to 80%. (iv) There should not be any GC clamp designed into any of the primers. (v) Primer length should fall into the range of 9 to 40 nucleotides. (vi) Hairpins with a stem length four or more residues should not exist in the primer sequence. (vii) Fewer than four repeated N homonucleotide residues should be present within a primer. (viii) The resulting amplicon should be at least 50 nucleotides in length but no larger than 100 nucleotides. (ix) The primers should be located toward the 3' end of the ORF. (x) In cases where predicted ORFs overlap, primers should be selected outside the region of overlap. However, it is important to note that until a complete transcript map for RRV is known, one cannot exclude the possibility that some primers are located in regions in which 3' untranslated regions (UTR) or 5' UTR segments of one gene overlap the ORF of an adjacent gene. Primers were designed using the PrimeTime program (W. Vahrson and D. P. Dittmer, unpublished data), based on European Molecular Biology Open Software Suite and Eprimer3, modules. The European Molecular Biology Open Software Suite (44) is a comprehensive collection of free open-source programs for sequence analysis. Eprimer3, is a program for searching PCR

primers and is based on the Primer3 program (46) from the Whitehead Institute/MIT Center for Genome Research.

Each experimental sample was analyzed as follows. RNA from RRV-infected RhFs was isolated using RNazol (Tel-Test Inc.) as previously described (16, 19). Poly(A) mRNA was prepared using dT-beads (QIAGEN Inc.) and reverse transcribed using Superscript II reverse transcriptase (Life Technologies Inc.) according to the manufacturer's recommendations. Five hundred nanograms of RNA was reverse transcribed in a 20- μl reaction volume with 100 U of Superscript II reverse transcriptase (Invitrogen Inc.), 2 mM deoxyribonucleoside triphosphates, 2.5 mM MgCl_2 , 1 U of RNasin (Applied Biosystems Inc.), and 0.5 μg of random hexanucleotide primers (Amersham Inc.). The reaction mixture was sequentially incubated at 42°C for 45 min, 52°C for 30 min, and 70°C for 10 min. Heating to 95°C for 5 min stopped the RT reaction. Next, 0.5 U RNase H (Invitrogen Inc.) was added and the reaction mixture was incubated at 37°C for an additional 30 min. Afterwards, the cDNA pool was diluted 25-fold with diethyl pyrocarbonate-treated, distilled H_2O and stored at -80°C . The forward primer and reverse primer sets were synthesized (MWG Biotech Inc.) and pipetted on separate plates. Individual primers were stored at 100 pmol/ μl at -80° , combined and diluted to yield enough forward and reverse primer mix for 100 reactions at a 267 nM final primer concentration. A 2.5- μl volume of primer mix was combined with 7.5 μl SYBR Green 2 \times PCR mix (Applied Biosystems Inc.) and 5 μl cDNA and subjected to real-time QPCR on an ABI5700 or MJR Opticon2 cyler using universal cycling conditions (see reference 37 for details).

Following the criteria outlined above, we initially computed three primer pairs for each predicted ORF in the RRV genome (data not shown). To ascertain the potential for nonspecific amplification and cross-reactivity to other herpesviruses, we conducted a National Center for Biotechnology Information (NCBI) BLAST search with each primer against (i) the RRV genome, (ii) all herpesvirus sequences in the GenBank database, and (iii) the human genome. The results are depicted in Fig. 1. For each individual primer (mean primer length, 20.33 nucleotides; 95% CI, 20.17 to 20.49; $n = 568$) the second closest alignment in the RRV genome contained, on average, 9.73 mismatches (95% CI, 9.55 to 9.91; $n = 568$), making it highly unlikely that any primer would anneal anywhere other than at its cognate sequence in the RRV genome. For example, a single primer that aligned perfectly at two different positions in the RRV genome (at nucleotide positions 115092 and 115023 in the RRV 26-95 genome) was eliminated from the array. The alignments for any RRV primer on any herpesvirus DNA segment in the NCBI GenBank database averaged 6.40 mismatches (95% CI, 6.16 to 6.64; $n = 568$). These matches were located in RRV genes homologous to other herpesviruses. Primers which showed ≥ 15 matches to any herpesvirus genome other than RRV were eliminated from the array and thereby enabled the specific detection of only RRV in samples containing other herpesviruses. Lastly, we compared all RRV primers against the human genome. The alignments for any RRV primer against the human genome averaged 4.11 mismatches (95% CI, 3.94 to 4.28; $n = 568$), which is statistically expected as the universe of possible target sequences increases by orders of magnitude (from $\sim 1.2 \times 10^6$

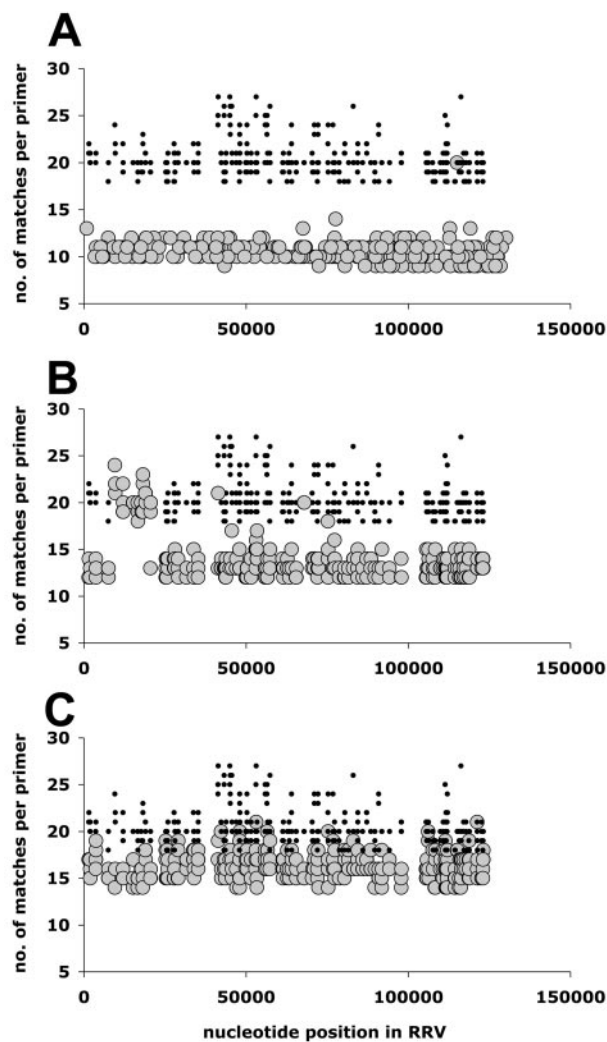


FIG. 1. RRV primer design and characteristics. Shown on the vertical axes are the numbers of nucleotide matches for each of the 568 primers in the initial RRV array, which contained three primers per ORF. On the horizontal axes, the nucleotide positions for each primer start site on the RRV genome (26-95) are indicated. In all three panels, A, B, and C, the small black dots represent the intended primer and numbered matches, which equals the primer length. In panel A, the large gray circles represent the second closest match for a given primer on the RRV genome. In panel B, the large gray circles represent the highest match for a given primer on any herpesvirus nucleotide sequence in the NCBI GenBank database, except RRV. In panel C, the large gray circles represent the highest match for a given primer on the human genome.

for all herpesvirus sequences to $\sim 10^9$ for the human genome). Only two primers (0.4%) exhibited a perfect match to a human DNA sequence, and these were removed from the array. We have shown previously that any ≥ 3 -nucleotide sequence difference can be recognized by dissociation profile analysis (38) and thus nonspecific amplification products would have been identified. No nonspecific amplification products were generated using the primer set listed in Table 1 (Fig. 2). To gauge the specificity and sensitivity of our approach, we conducted the following quality control experiments. (i) The cDNA was subjected to PCR with the primer pairs shown in Table 1. We analyzed the PCR products by agarose gel electrophoresis and

found that every primer pair in the RRV array yielded a single product of uniform size (Fig. 2A). (ii) We conducted melting curve analysis for every experiment (data not shown) and excluded data for primer pairs which did not yield a single peak dissociation profile from further analysis. (iii) Under the stringent real-time QPCR conditions used (60°C annealing temperature, 60-s extension phase), no primer in the RRV array yielded a signal using either KSHV- or Epstein-Barr virus-infected cell mRNA as the target sample (data not shown).

Figure 2B shows the unmanipulated cycle number (CT) signals for each primer using the following samples as targets: (i) water, as a nontemplate control (NTC; open squares), (ii) RNA from uninfected cells that was DNase I treated, reverse transcribed, and RNase H treated (gray circles), (iii) RNA from uninfected cells that was DNase I treated but prepared without reverse transcriptase in the cDNA reaction and subjected to RNase H digestion (gray squares), and (iv) RRV virion DNA (gray line). Only cDNA from RRV-infected cells or RRV virion DNA yielded a significant signal. The positive signal was, on average, 15.84 CT units (95% CI, 14.86 to 16.81) or $2^{\text{CT}} = 58,656$ -fold above the background of the mock-infected, the RT-negative, or the NTC sample. This outcome demonstrates that the primer pairs were specific for RRV mRNAs, not cellular mRNAs. This experiment verified our contention that even if an individual primer showed limited similarity to a cellular gene (Fig. 1), the chance of both 20-mer primers in a primer pair containing significant sequence identity to the same cellular gene and being located in close enough proximity ($\leq 1,000$ bp) to be amplified during the 60-s extension phase of the real-time QPCR protocol is infinitesimal. Furthermore, we confirmed that our mRNA/cDNA preparations did not contain contaminating viral DNA (Fig. 2B). In certain reactions, the NTC target yielded a higher background signal than cDNA from mock-infected cells, which is not unexpected, since even unspecific nucleic acids have a quenching effect on the PCR, thereby affecting overall PCR efficiency. Ten of the initial 83 (12%) RRV-specific primers did not amplify virion DNA or cDNA from productively infected cells (data not shown). These “primer failures” were replaced with alternative primers in subsequent experiments (Table 1 depicts only the experimentally validated primer pairs for RRV). For all primers, the virion DNA target yielded a mean CT of 24.41 (95% CI, 23.41 to 25.41; $n = 72$). In other words, any change in CT of ≥ 1 could not be attributed to differences in primer efficiency but was due to changes in target mRNA. Figure 2C plots the standard deviation (SD; $n = 5$) relative to the mean CT for each gene in the RRV array. Note that Fig. 2C, is on a \log_2 scale. Five CT units represents a 32-fold change, and 10 CT units represents a 1,024-fold change in relative mRNA levels. There was no significant correlation between the magnitude of the SD and the mean CT ($r = 0.31$; $n = 82$), demonstrating that changes in RRV gene expression did not depend on the overall levels of any particular viral mRNA (Fig. 2C).

RRV transcription upon de novo infection of fully permissive RhFs. To chart the transcription profile of a rhadinovirus upon primary infection of highly permissive cells, we infected RhFs with RRV at a multiplicity of infection (MOI) of 1, and isolated mRNA at different time points after viral infection. The mRNA pools were reverse transcribed using hexamer

TABLE 1. Real-time QPCR primers for the RRV array^a

Well	Name	Forward primer sequence	T _m (°C)	Position	Name	Reverse primer sequence	T _m (°C)	Position
A1	R-ORFR1-1f	GACCGCAGGAAAAACAATTA	60	1495	R-ORF1-2r	CCATGTGCTCAACATTATCCTC	59	1575
A2	R-ORF2-1f	ACGCGCATTATGGAGAGTTT	60	1991	R-ORF2-2r	TTGTATCTTTGCCCGGTAGC	60	1914
A3	R-ORF4-1f	CAATAGCACCCCAATGAGT	60	3670	R-ORF4-2r	CAATAAAGGGCAGCAAGTACG	60	3746
A4	R-ORF6-1f	ATATCGCCACCGCTTCCCT	61	7493	R-ORF6-2r	CTCAGCAGCGCGTTAAATTTT	61	7576
A5	R-ORF7-1f	CCTGTATCTAACGTACGAGCAAGA	60	9567	R-ORF7-2r	TGCAGGTGATGGTACAGAAGA	59	9648
A6	R-ORF8-1f	CCGGTTAGACGAAACAGCAG	60	12043	R-ORF8-2r	CTTCGTTTTCCAGCGGTTTA	60	12124
A7	R-ORF9-1f	ACCCGGATTACGTACAGACAG	60	15165	R-ORF9-2r	CCGAACAGACACTGGAGGAT	60	15245
A8	R-ORF10-1f	CATTAACCGCGTTCACAATCC	59	16577	R-ORF10-2r	CAATGGTTCATGCGTTCGT	61	16660
A9	R-ORF11-1f	CCGAACCGGGAGATAGAGAT	60	17684	R-ORF11-2r	CGAACACGAAGATGGCTTG	60	17762
A10	R-ORFR2-1f	GGAGCTTCCCGTAAATAACAAG	59	18233	R-ORFR2-2r	GAAACGCGCTGAGAACAAC	60	18151
A11	R-ORF70-1f	GCGGCTGAAGATTTTGAGAA	60	19037	R-ORF70-2r	GCCATCTCCATCTCTATGTGG	60	18952
A12	R-ORFR4-1f	GGACGACGAGTGAAGAAAC	61	20570	R-ORFR4-2r	CGTTGGAAGCATCGTCAAT	60	20495
B1	R-ORF16-1f	AATGGGAGGGCTCAGGAAT	60	25224	R-ORF16-2r	CCTAGCGCCAGAGACCA	60	25309
B2	R-ORF17-1f	CCGCCAAGAATCTGTAATG	60	25616	R-ORF17-2r	GGACTGTCCGCATTCTGG	60	25541
B3	R-ORF18-1f	AGTGTGTCGCGATGTTCC	59	27719	R-ORF18-2r	CGCAAACAAGTAGTCCGCTCG	61	27798
B4	R-ORF19-1f	ACCAAAGCTCACGTTCCAGG	60	28045	R-ORF19-2r	GATGGGTGCGAGAGGATG	60	27962
B5	R-ORF20-1f	CGCGTTCGTTGTCACAATAG	60	29097	R-ORF20-2r	AGCCATTGGTTTTGGTTCAT	59	29012
B6	R-ORF21-1f	TATGGGCAGGTGATGTCAAAA	60	31599	R-ORF21-2r	CATTGCTTTCCAAGCTGGTT	60	31679
B7	R-ORF22-1f	TTGTACAGAAGACACGCACTCA	60	33772	R-ORF22-2r	TAGGCCAGGATGGAAAACAG	60	33856
B8	R-ORF23-1f	GAGAGCTGGCCATTCAAGTT	59	34008	R-ORF23-2r	TACGCGGGACTGAGATTAG	60	33933
B9	R-ORF24-1f	CGCAACGCCAATTTTATGT	60	35238	R-ORF24-2r	CCAGTGAAGTCCCAAACGTC	61	35152
B10	R-ORF25-1f	TGGACGAATATATGTGCAATAAGC	59	41349	R-ORF25-2r	TCCGATCTTTAATAGTCTTTTCATAGG	60	41423
B11	R-ORF26-1f	TGCCCTATGACCTATCTACG	60	42299	R-ORF26-2r	AACAGGAAGCGGTATTCGTG	60	42380
B12	R-ORF27-1f	CCCCACCTGGAATGATGTA	59	43142	R-ORF27-2r	GCATCACCATTAAGCACTATTACAC	59	43222
C1	R-ORF28-1f	ATGCGGAGGGTGTGTTGTA	60	43578	R-ORF28-2r	GGACGCAACCTAACATTCA	61	43654
C2	R-ORF29b-1f	CTAAAAGCGGAGGTACACG	60	43846	R-ORF29b-2r	TCGTTGGTTGCCATGTAGTG	61	43769
C3	R-ORF30-1f	TTTAAACCACTTTAGCCTATCTGAATC	60	45020	R-ORF30-2r	GCGATCGTGGTATAAGAGAGACA	61	45102
C4	R-ORF31-1f	TCCCATATACTCCACTAAAACGGTA	59	45594	R-ORF31-2r	CATCCATTGCGCTCTGATAG	59	45678
C5	R-ORF32-1f	AGCGGGCAGTCTACTGTTTG	60	46927	R-ORF32-2r	AGGTCGTAGCGGCTTTAAT	60	47002
C6	R-ORF33-1f	GTGCAACCCACTTCGCTAC	59	47957	R-ORF33-2r	AGCAGATGCTTTTAAAGTCTGCG	59	48031
C7	R-ORF29a-1f	GGCGAAGAACCTGAACATAAA	59	48139	R-ORF29a-2r	TATTGAAGCACGTCGCACAC	61	48062
C8	R-ORF34-1f	ACGTCTAGTGTTCGGGCTCA	61	49834	R-ORF34-2r	GAGGCCATGTTCCCTTATCA	60	49919
C9	R-ORF35-1f	AGCTGTACGGGAGACTGGAGAT	59	50247	R-ORF35-2r	GACGCTCCAATTTCCACCTA	60	50332
C10	R-ORF36-1f	CGGTTAGAAAACGCATCCCTC	60	51468	R-ORF36-2r	GCAAGTTCCGCAATGACTAAA	60	51546
C11	R-ORF37-1f	AAACACCAACTGGTGAAGCA	59	52900	R-ORF37-2r	GCGTTTGACACAGAGAGG	61	52982
C12	R-ORF38-1f	AGGAGAAGAAAGCATTTGCTTGTTA	60	53066	R-ORF38-2r	TGACAAATTTATGTTTTATGTTTGGGA	60	53142
D1	R-ORF39-1f	TCCTCAAGGCCCTAAAGAGAA	60	53360	R-ORF39-2r	CCTCGTAATCGTCACTGCT	60	53286
D2	R-ORF40-1f	GCGGCCATTGATAAAAACAAC	60	55827	R-ORF40-2r	TTTCTACGGCAACTATTTAGTGA	59	55899
D3	R-ORF41-1f	CCTACAGGAGGCATATGTTGTTT	60	56422	R-ORF41-2r	CCTTTTCAAACCTTCTAATTTGTCG	60	56495
D4	R-ORF42-1f	TTTTATTGCGGACAAATTTTT	60	56617	R-ORF42-2r	AGTTTGTCTGGGATGCTGT	60	56542
D5	R-ORF43-1f	CCAGCTGTATGTGGACAGCA	61	57418	R-ORF43-2r	GCTTCAGTATTTGGTCCATCG	60	57333
D6	R-ORF44-1f	GGACAGCAACCCCTTAAA	60	61241	R-ORF44-2r	GAGGGTGTGTTTGGGTTGT	60	61318
D7	R-ORF45-1f	GGGGCTACTTCTAACCCAGAG	59	61474	R-ORF45-2r	GGCCACGGATAGTTGTCATT	60	61400
D8	R-ORF46-1f	TTCTGCCAAGCTTCAGAGGT	60	62714	R-ORF46-2r	CGCTTGGAGACGAGCTC	61	62633
D9	R-ORF47-1f	AGCTGTGCCGACTTAACC	60	63317	R-ORF47-2r	TGTCTCGAGCCAAGTATCCA	59	63240
D10	R-ORF48-1f	ACGAGGGTATCTGGACTCA	60	64066	R-ORF48-2r	CTAAGCTCCTCAAAGACAATTTCC	60	63989
D11	R-ORF49-1f	AGCACTGTCCGAGCACTA	61	65468	R-ORF49-2r	GATTGAGGAGGCGTGTITA	60	65392
D12	R-ORF50-1f	AAAACGACGACGACATGCTA	59	67876	R-ORF50-2r	TCCTCATTGTCCGAGTTGCT	61	67956
E1	R-ORF52-1f	AATGGACGAGACCAACAGAG	60	70467	R-ORF52-2r	AGTCCCGCTGCTTATTTCTG	60	70389
E2	R-ORF53-1f	ACGCCCTCTTTTTATGACTATGA	59	71018	R-ORF53-2r	CGCGACCAGAACAGAGTTG	61	70939
E3	R-ORF54-1f	GGCACCTCCCTCCAGATA	60	71980	R-ORF54-2r	TTCGGTTTGGCTTTGAGTGT	61	72065
E4	R-ORF55-1f	GTAGACACCGAAGCGTCCCTC	60	72296	R-ORF55-2r	CTGTATATTTTGTCTGGCACGA	59	72214
E5	R-ORF56-1f	TCCAAAAAGAAAGCGAGGT	60	75207	R-ORF56-2r	TGGGTACCATAAATGAAAAATGTG	60	75286
E6	R-ORF57-1f	CTTAAATTC AATAGTGGTGGAGCA	60	76772	R-ORF57-2r	CCTGTTGTTTTCCGCCAGT	60	76850
E7	R-ORFR9-1f	ATCCGTTTGCACAGATTTGG	61	77348	R-ORFR9-1r	TATTTACGCTGGTGGACAA	60	77270
E8	R-ORFR9-2f	AGAGGGGACGAGCCAATC	60	78772	R-ORFR9-2r	ATCATCTTACCCGCTCGTTC	60	78690
E9	R-ORFR9-3f	TTTGGGGCGTACTTACA	60	80335	R-ORFR9-3r	AACATTAGCGCGGACAA	60	80248
E10	R-ORFR9-4f	ACGGGGCAACACTGTATCTC	60	81582	R-ORFR9-4r	GTGTCCCTGCACCAGCTC	60	81501
E11	R-ORFR9-5f	AACTGTGGGTTTCGGGTTGT	61	83120	R-ORFR9-5r	TCAAAGTGCTATAGATTTCTGTTTG	60	83040
E12	R-ORFR9-6f	ATGTGTCAGATGATGTCAGCAA	59	84455	R-ORFR9-6r	AGATGTGCTTCCCGTTGTTTC	60	84373
F1	R-ORFR9-7f	GATTTCCAGCCGCTATG	59	85998	R-ORFR9-7r	GCCAAATTTGAATGGACAGG	60	85920
F2	R-ORFR9-8f	CGCAGTCACTCTTTACCTTGG	60	87213	R-ORFR9-8r	GTCACCATGAGTCAATTCATCC	59	87134
F3	R-ORF58-1f	GCGAAGCTCGCCAGGAATAGT	59	88529	R-ORF58-2r	TAAAGGGCACCAAGCTCAAC	60	88448
F4	R-ORF59-1f	GAACGCTGACCTGAGACTTA	60	89723	R-ORF59-2r	GCTCGTCCGAGTATTT	60	89648
F5	R-ORF60-1f	CAAACCGCTGTCCCTTGT	61	90933	R-ORF60-2r	CAGATCATTATGAACGGATGTGA	60	90856
F6	R-ORF61-1f	ATGCCTGCAAGTGTCTTAGAT	60	91878	R-ORF61-2r	ACATACCTTGGTCCGCTCAC	60	91794
F7	R-ORF62-1f	CTTCCCGTGTCAACCATCT	60	94241	R-ORF62-2r	CTTCCAAGACCCCGATT	60	94160
F8	R-ORF63-1f	TGTCGATGATTTGGAGCACAA	60	97852	R-ORF63-2r	GCAAACATGCGATCTAGTGC	59	97935
F9	R-ORF64-1f	AAGAAATCACACGAGCCAAGA	60	105490	R-ORF64-2r	CTGGCAATAGCCTCGGATAG	60	105570
F10	R-ORF65-1f	GGGCCCAATTCATGTATAG	60	105759	R-ORF65-2r	CGTAGGTTGATAACGAAAGTGG	60	105675
F11	R-ORF66-1f	ACCGAACTCCTGGTTAG	60	106267	R-ORF66-2r	ATAAAACAGCTACGCCACAC	60	106188
F12	R-ORF67-1f	GAACGGTTTTTGCCTGAC	60	107623	R-ORF67-2r	CGCCCAATATCCTTCAACTC	60	107538

Continued on following page

TABLE 1—Continued

Well	Name	Forward primer sequence	T _m (°C)	Position	Name	Reverse primer sequence	T _m (°C)	Position
G1	R-ORF67-5f	CACTGTGAGCACTGCATGG	60	108293	R-ORF67-2r	CGTGGCTCCCCTAAAAAC	59	108213
G2	R-ORF68-1f	GGTCTCAACTGGCCAAAATC	60	109845	R-ORF68-2r	GGGTGGGTGATTTGAATGTT	60	109922
G3	R-ORF69-1f	TAACGGTGGACTGCATCAAG	60	110700	R-ORF69-2r	CCTCGCAAATGCTGTTGAC	60	110780
G4	R-ORF71-1f	CAACCAGTCACCCACCTTTT	60	117122	R-ORF71-2r	TGCAGCAGGTCACTTAAAACC	60	117046
G5	R-ORF72-1f	CCAGGTGGTGGAGTCTGTTC	61	117798	R-ORF72-2r	GCACCGAGGCTAAACAGC	60	117716
G6	R-ORF73-1f	TCACGGTGTCTGTCAAAGC	60	118766	R-ORF73-2r	CTATGCTGGCCTGGAAGTG	59	118681
G7	R-ORFR14-1f	CACGTGCCTGGTCACTCATA	61	121242	R-ORFR14-2r	CACCACGTAGTGGCTCGTC	60	121320
G8	R-ORF74-1f	AGCATGTATAGCGCGTTCGT	61	122616	R-ORF74-2r	AAAACACCTAAACACGGACCA	59	122691
G9	R-ORF75-1f	CCATCTCAACCAGCAGCAG	61	123101	R-ORF75-2r	GAGTTGGCAGACGGGTTG	60	123018
G10	R-R8-1f	AAACGCAACACTCGGACAC	60	68932	R-R8-2r	TGTTTTACTTCCAGTCTCTGTT	59	69163
G11	R-R15-1f	TTGCTGCAATGTGTATGGCC	63	128129	R-R15-2r	TTGCAACATAACAAACAAGCATGT	62	128072
G12	No primer							
H1	hu-gapdhf	GAAGGTGAAGGTCGGAGTC	57	NA	hu-gapdh-f	GAAGATGGTGATGGGATTTTC	57	NA
H2	hu-actinf	TCACCCACACTGTGCCATCTACGA	72	NA	hu-actin-f	CAGCGGAACCGCTCATTGCCAATGG	77	NA
H3	mu-apoBf	TCACCAAGTCAATTTCTGCCTTTG	63	NA	mu-apoBr	CACGTGGGCTCCAGCATT	63	NA
H4	rh-tub P2f	CCCTTCCCACGCCTCC	63	NA	rh-tub P2r	GGCTTCCACGGCTGGTG	64	NA
H5	KSHVLAT273f	ACTGAACACACGGACAACGG	62	NA	KSHVlat335r	CAGGTTCTCCCATCGACGA	62	NA
H6	KSHVorf72f1	CATTGCCCGCTCTATTATCA	62	NA	KSHVorf72r1	ATGACGTTGGCAGGAACCA	63	NA
H7	KSHVorf50f	CACAAAAATGGCGCAAGATGA	64	NA	KSHVorf50r	TGGTAGAGTTGGGCCTTCAGTT	62	NA
H8	KSHVorf57f	TGGACATTATGAAGGGCATCCTA	63	NA	KSHVorf57r	CGGGTTCGGACAATTGCT	62	NA
H9	KSHVK1-f	AAACAACGTGACTCAAACAAAACA	61	NA	KSHVK1r	TCTTCCGTGCACAAATCGTG	63	NA
H10	KSHVvGPCRf	TGGCCCAAACGGAGGATCCTAG	68	NA	KSHVvGPCRr	AGTTTCATTCCAGGATTCATCATC	61	NA
H11	KSHVLANA2454f	TGGCCCATCTCGCAATA	64	NA	KSHVLANA2524R	GCCTCATACGAACTCCAGGTCT	62	NA
H12	Rh-tubP2f	CCCTTCCCACGCCTCC	63	NA	rh-tubP2r	GGCTTCCACGGCTGGTG	63	NA

^a Listed are the forward and reverse primer sequences, primer name, position on the RRV genome, and predicted T_m for each well in the 96-primer RRV array. NA, not applicable.

primers and subjected to real-time QPCR using the RRV array. During real-time QPCR, the amount of product at each cycle is quantified (23) and the CT at which the product signal crossed a user-defined threshold is recorded, which was set here at five times the SD of the nontemplate control reaction.

The RRV array recorded duplicate measurements for the rhesus tubulin mRNA-specific primers for each time point. The levels of rhesus tubulin exhibited a SD of ≤ 1.7 -fold with an associated standard error of the mean (SEM) of $\pm 4\%$ for all time points ($n = 5$). Replicate measurements of the rhesus tubulin mRNA for any one time point on the same array also exhibited an SEM of $\pm 4\%$ in raw CT values, which was expected based on the pipetting accuracy of the robot and the instrument variation of the real-time QPCR machine (38). By contrast, viral mRNAs increased, on average, 5,379-fold (95% CI, 3,154-fold to 7,604-fold; $n = 83$) based upon a conservative estimate of PCR efficiency of 1.8, rather than the ideal 2.0. Hence, we concluded that for any target in the array, the biological variation was orders of magnitude above the experimental error.

All samples were highly correlated, with an average correlation coefficient $r = 0.961 \pm 0.021$ (mean \pm SD) for all possible sample correlations (Fig. 2D). Any two consecutive time points (e.g., 12 and 24 h or 24 and 48 h) were more closely correlated than unrelated time points (e.g., 12 and 48 h), indicating a progressive, gradual change in overall viral transcription. This substantiated the existing model of an ordered cascade of herpesvirus gene expression after a high MOI of fully permissive cells. It represents the first and only such demonstration for primate gammaherpesviruses, since neither KSHV nor Epstein-Barr virus currently has a highly efficient, fully permissive lytic replication system, without the use of chemicals like TPA. Kinetics of gene transcription for MHV-68, a murine gammaherpesvirus, has been determined (45). For

KSHV, we and others have reported the whole-genome transcription patterns upon reactivation in lymphoma cell lines (19, 25, 39, 48, 59), with estimated reactivation frequencies of 5 to 30%, depending on the particular virus and cell line used. Krishnan et al. (28) have recently reported the induction of a limited set of lytic and latent viral genes immediately following KSHV infection of endothelial cells and fibroblasts. However, the full lytic program was only observed after TPA addition to the infected endothelial cells 48 h postinfection (28), demonstrating the predilection for KSHV to enter the latent phase of its viral life cycle in current tissue culture systems. Hence, the ability of RRV to fully replicate in RhFs and exhibit a progressive, gradual, and ordered change in viral transcription (in the absence of TPA, which might activate multiple viral promoters and hence skew the transcription profile) is important to demonstrate the ordered kinetics of gammaherpesvirus gene expression.

Microarray studies hinge upon the correct method of analysis. Therefore, we will briefly justify the approach we used for our analysis before presenting the experimental outcome. We employed several different means of statistical analysis, all of which yielded astonishingly congruent rank orders. To determine coregulated clusters of mRNAs purely upon their pattern of induction, the raw CT values were subjected to hierarchical clustering using euclidian standard correlation or a Pearson correlation-based metric. Euclidian clustering calculates distances between two datum points based on the sum of square differences (Fig. 3A). The scale encompasses the lowest level of the mRNA of overall lowest abundance (black) in the entire array to the highest level of the mRNA of overall highest abundance (red). Hence, information about overall mRNA levels strongly impacts the rank order, and even background levels exert considerable influence (This is the reason for the weak signal at $t = 0$ in Fig. 3A.) If the array comprises a range

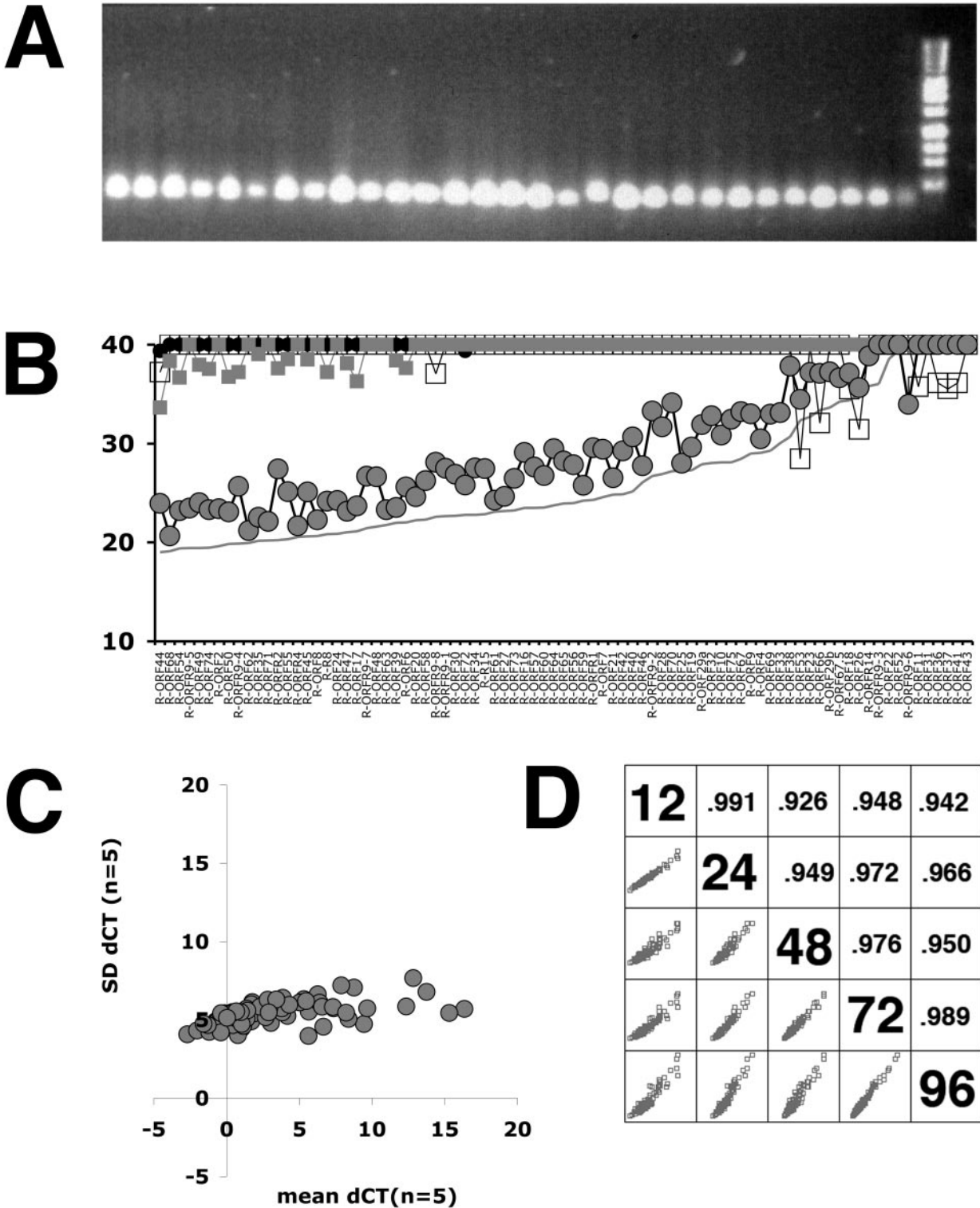
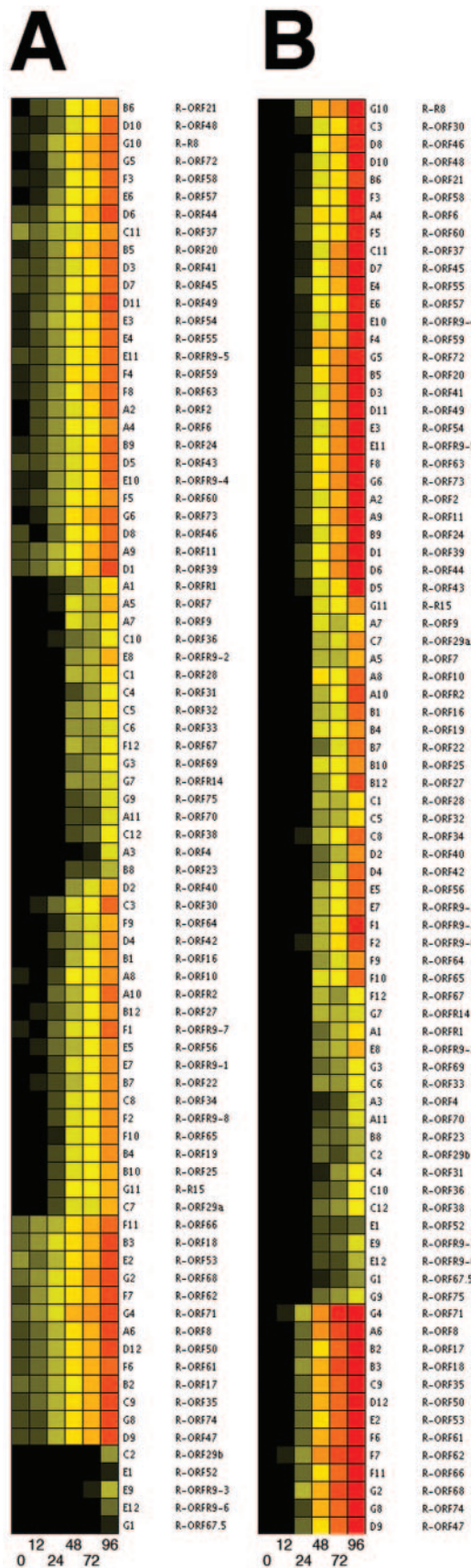


FIG. 2. Quality control of the RRV RT-PCR array. (A) Agarose gel of a subset of PCR products after amplification of RRV virion DNA with primers in the RRV array. A 100-bp molecular weight marker is shown on the right. (B) Raw CT values after real-time QPCR using the following input samples: (i) water as an NTC (open squares); (ii) RNA from uninfected cells that was DNase I treated, reverse transcribed, and RNase H treated (gray circles); (iii) RNA from uninfected cells that was DNase I treated but prepared without reverse transcriptase in the cDNA reaction and subjected to RNase H digestion (gray squares); and (iv) RRV virion DNA (gray line). (C) RhFs were infected with RRV at five different time points ($n = 5$), 12, 24, 48, 72, and 96 h. mRNAs were harvested and subjected to real-time RT-PCR. The dCT values of RRV mRNAs were normalized to that of rhesus tubulin. Panel C is a graph representing the SD of the dCT values (vertical axis) versus the mean dCT values (horizontal axis). Lower dCT values correspond to higher levels of mRNA on a \log_2 scale (dCT). (D) Scatter plot matrix of raw CT data for each time point after productive infection of RhFs with RRV depicted as a diagonal line. Also shown is the correlation coefficient for each pair of datum sets.



of RNAs of very different abundances, such as the housekeeping genes for glyceraldehyde-3-phosphate dehydrogenase and actin and rRNAs in addition to low-abundance viral RNAs, changes in the low-abundance mRNAs will contribute to clustering but will not be visible in the color scheme. A standard-correlation metric based clustering calculates the distance as the arc cosine of the scalar product with a maximal range of ± 1 . By definition, genes with all measurements of zero (i.e., the gene for rhesus tubulin, the normalizing gene) are excluded. This metric compresses the range to yield a unit length normalization but maintains a more realistic representation of mRNA levels among different transcripts. Finally, Pearson correlation-based clustering rescales and median centers the data such that for each gene the time point with the highest-abundance mRNA is set to 1 and the lowest to -1 , regardless of overall levels for individual mRNAs. This approach to data analysis yields a relative rank ordering of mRNAs based solely upon their pattern of changes. Two genes with widely different absolute mRNA levels will group together if their transcription patterns change in a similar fashion. This metric is directly comparable to information that can be gathered from Cy3/Cy5 comparative hybridization-based microarrays (18).

Real-time QPCR-based analysis also allowed us to exclude the variation in total RNA levels and reverse transcriptase efficiency of a particular sample by calculating the abundance of a given RRV mRNA relative to the level of a cellular gene. Here we used rhesus tubulin (RhTub) as $dCT = CT_{\text{gene}} - CT_{\text{RhTub}}$, to normalize for viral gene expression as reported in previous publications (16, 19, 32, 40, 41, 54). These dCT values were then subjected to cluster analysis. We applied hierarchical clustering as previously described (18) using ArrayMiner software (OptimaDesign Inc.) under Macintosh OsX10.3.4 (Apple Inc.). ArrayMiner uses Gaussian clustering (a genetic algorithm) as an alternative to self-organizing maps or k means clustering. Both methods yield concurrent results for highly correlated genes that change in a specific pattern, but Gaussian clustering allowed us to identify outliers, namely, genes with no recognizable pattern of transcription. By contrast, distance-based methods always force all signals into an apparent rank order, even if there is no correlation between adjacent entries. Additional calculations were performed using Excel (Microsoft Inc., Redwood, WA) and SPSS v11.0 (SPSS Science Inc., Chicago, IL). Note that the dCT values are still \log_2 derivatives of the underlying mRNA levels and that clustering using a correlation metric is insensitive to differences in individual primer efficiency (see references 17 and 37 for discussions).

Taking into account the level and pattern of transcription, we obtained distinct clusters of genes after RRV infection of fully permissive RhFs. Five different time points were employed: 12, 24, 48, 72, and 96 h postinfection. None of the RRV

FIG. 3. Whole-genome profiling of RRV transcripts following de novo infection of RhFs. (A) Shown is a heat map representation of real-time QPCR data normalized to rhesus tubulin (dCT) at 0, 12, 24, 48, 72, and 96 h postinfection of permissive RhFs. Black indicates low, yellow represents intermediate, and red represents the highest level of viral mRNA detected. Panel A shows the result of rank ordering using a euclidian matrix. (B) Result of rank ordering using the scalar product of mRNA levels normalized to rhesus tubulin.

mRNA levels decreased at late time points (40, 41). Between 72 h and 96 h after RRV infection, cellular mRNAs (tubulin, actin) decreased ≥ 10 -fold since many cells in the population start to die and only cells that were intact were used for analysis. By definition, these cells would not have completed the viral life cycle, which destroys the host cell. Individual RRV mRNAs differed based upon how early significant levels (black-to-yellow transition) could be detected. During the course of the infection, the levels of the RRV mRNAs reached the level of tubulin mRNA in the cell (mean, 1.01-fold; 95% CI, 0.72-fold to 1.3-fold; $n = 415$). Thus, RRV mRNAs were easily detectable and yielded a very robust signal in the middle of the linear range of the real-time QPCR assay.

Figure 3 shows the relative abundance and change in transcription of each RRV mRNA based upon a euclidian (panel A) or a correlation-based (panel B) metric. ORFs 50, R8, 66, 8, 17, 18, 35, 47, 53, 61, 68, 71, and 74 were transcribed at the earliest time point (12 h) after infection and accumulated to the highest levels. For this group, changes in RRV transcription averaged 1,417-fold (95% CI, 983-fold to 1,850-fold; $n = 15$) between 12 and 96 h postinfection and RRV mRNA levels climbed from 0.05-fold over tubulin mRNA levels (95% CI, 0.03-fold to 0.09-fold; $n = 15$) at 12 h postinfection to 65-fold over tubulin mRNA levels (95% CI, 53-fold to 77-fold; $n = 15$) at 96 h postinfection. This occurred exponentially (fold = $0.0048 \times e^{0.098 \times \text{time}}$). Of note, this clustering cannot be attributed to primer efficiency since primers for these mRNAs do not group together if viral DNA is used as a target (Fig. 1B). The early group of viral genes expressed within 12 to 24 h postinfection included ORF50, the RRV immediate-early transactivator (11, 12), as well as RRV R8, another early gene in RRV (12) (Fig. 3B). In addition, RRV genes ORF35, -61, and -74 were also induced early (Fig. 3A and B). A comparison with the transcription patterns for KSHV genes shows that the homologs of these RRV genes in KSHV (ORF50/Rta, K8/bZip, ORF35, ORF61/ribonucleotide reductase, ORF74/vGPCR) were also significantly induced as early as 10 h after reactivation (19, 25, 39). For these genes, the amino acid sequence and transcriptional regulation are conserved between KSHV and RRV, even though they encompass a wide range of differing biological functions. Other early RRV genes in this cluster included ORF17, -18, -53, and -66 (Fig. 3A and B), which yielded a strong signal at 24 h after infection and whose KSHV homologs were also significantly induced at 24 h after KSHV reactivation and hence represent the first wave of transcripts for both viruses (19, 25, 39).

The mRNA for ORF71/vFLIP is differently regulated between RRV and KSHV. In RRV, primary infection of RhFs resulted in early expression of ORF71/vFLIP, whose expression increases 1,249-fold from 0 to 96 h (Fig. 3A and B). By contrast, KSHV ORF71/vFLIP mRNA levels do not significantly change upon viral reactivation (16, 19). The RRV ORF72/vCyclin and ORF73/LANA mRNAs were also induced during the course of RRV de novo infection and increased 2,588-fold and 3,217-fold by 96 h postinfection, respectively. The RRV ORF71, -72, and -73 gene expression profiles also grouped with mRNA transcripts for RRV genes including ORFs 2, 6, 11, 20, 21, 24, 37, 39, 41, 43, 44, 45, 46, 48, 49, 54, 55, 57, 58, 59, 60, 63, R9-5, and R9-4 (Fig. 3A and B). These transcripts appeared at 24 h postinfection but increased most drastically

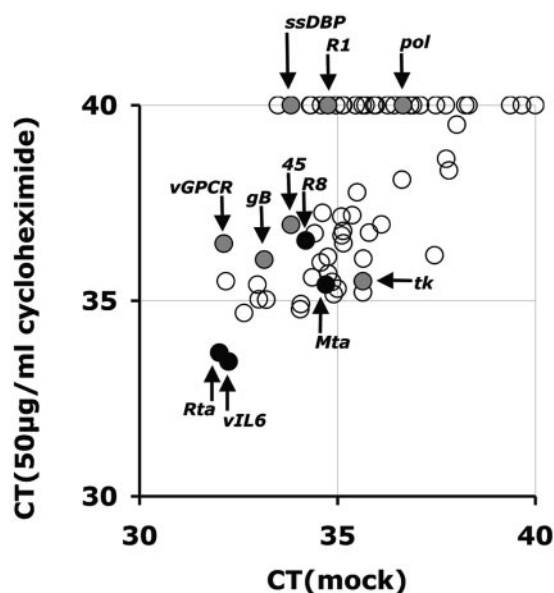


FIG. 4. Impact of cycloheximide on RRV transcription. RhFs were pretreated with 50 $\mu\text{g/ml}$ cycloheximide for 1 h, infected with RRV at an MOI of 1, and maintained in cycloheximide until the end of the experiment. Plotted are the CT values for all RRV mRNAs in the array at 6 h after infection in the presence (vertical axis) or absence (horizontal axis) of cycloheximide. Black circles represent mRNAs that are immediate-early genes in KSHV, gray circles represent genes that are known transcriptional targets of ORF50/Rta, and open circles represent all other RRV mRNAs.

between 48 and 72 h and therefore were grouped separately (fold = $0.0004 \times e^{0.113 \times \text{time}}$). The transcription pattern for this group of genes also paralleled the temporal regulation of their KSHV counterparts (19, 25, 39). An exception is RRV ORF4/complement binding protein, which is significantly induced at 24 h after reactivation in KSHV but could not be detected until 72 to 96 h after de novo infection of RhFs with RRV. The mRNAs for ORFs 23, 31, 36, 52, R9-3, and R9-6 also clustered together and did not accumulate to significant levels until 96 h postinfection and were thus considered late genes.

In order to distinguish the immediate-early genes from the early and late transcripts, we performed RRV infections of RhFs in the presence of cycloheximide. RhFs were pretreated with cycloheximide at 50 $\mu\text{g/ml}$ for 1 h, infected with RRV in the presence of drug, and kept in cycloheximide until the time of harvest. Cells were harvested at 6 and 12 h postinfection (in the presence or absence of drug), and total RNA was isolated. The RNA was subjected to array analysis as described above. Due to the facts that different cell lines exhibit different sensitivities to cycloheximide and most die by 24 h (58), we report our data as raw CT values in a two-dimensional correlation analysis (Fig. 4). We were able to identify groups of RRV transcripts that were differentially regulated by cycloheximide (data not shown). (i) Late genes were not transcribed in the presence or absence of drug at 6 and 12 h. These are ORFs 4, 25, 28, 29b, 32, 36, 38, 53, R9-3, 65, 67, 67.5, 69, 75, R9-6, 23, and 9. For these, the CT cycle numbers were ≥ 38 (i.e., ≤ 4 -fold above background) at three of four samples points. (ii) Early genes were significantly transcribed at 6 h p.i. and strongly

inhibited by cycloheximide. Hence, they appear shifted upward of the 45° line in Fig. 4. These are ORFs R1, 70, 2, 43, 6, 29a, 17, R9-1, 27, 24, 45, 55, R8, 74, 8, and 49. Interestingly, this set includes many of the genes that are known to be regulated by ORF50/Rta (11) in KSHV, namely, ssDBP/ORF6, R1, DNAPol/ORF9, gB/ORF8, vGPCR/orf74, and ORF45 (Fig. 4, gray circles). RRV TK/ORF21 was transcribed at low levels at 6 h and inhibited by cycloheximide at 12 h (data not shown). (iii) Based on our analysis, we classify RRV Rta/ORF50 and vIL6/ORF2 as the most highly induced and cycloheximide-resistant immediate-early genes in RRV. At 6 h, these two genes were transcribed at approximately 8- to 10-fold higher levels than Mta/ORF57, which also was resistant to cycloheximide treatment. The RRV R8 gene was slightly sensitive to cycloheximide, suggesting that it is dependent on Rta/ORF50 to a slightly higher degree than KSHV Zta/R8, which has been reported as an immediate-early gene (60) but also as a delayed-early and Rta/ORF50-responsive gene (56). (iv) Finally, we identified a number of RNAs that are transcribed at 6 h postinfection, but to a lesser degree than Rta/ORF50, and show intermediate inhibition (fivefold or less) to cycloheximide (data not shown). These can be classified as early genes on the basis of timing, but their promoters are less stringently dependent on viral immediate-early transactivators. Whether this is biologically relevant or whether the promoters are simply leaky in the context of drug treatment remains to be determined.

We have previously reported that RRV replication is sensitive to phosphonoacetic acid (PAA) (12). RhFs were infected at an MOI of 1 in either the presence or the absence of 50 μ M PAA, and viral transcription profiles were determined at 12, 24, and 48 h postinfection (Fig. 5). To exclude possible drug effects on the cellular genes, we plotted the raw CT values (higher values correspond to lower abundances). At 12 h, no effect of PAA was discernible and the RRV mRNA levels in the absence of PAA were identical to the RRV mRNA levels in the presence of PAA, as demonstrated by linear regression analysis with $r^2 = 0.9262$ and $m = 0.9959$, i.e., 45° (panel A). This outcome was consistent with the mechanism of action of PAA, which inhibits the viral polymerase but does not interfere with immediate-early and early transcription (53, 61). At 24 h, none of the mRNA levels were inhibited more than threefold in response to PAA. At 24 h, PAA inhibited RRV transcripts under both high-MOI and low-MOI conditions (Fig. 5B and F), specifically, ORFs7, 9, 19, 28, 29b, 32, 34, R9.2, 59, and 67. At 48 h, the effect was more pronounced (Fig. 5C and G) and in particular ORFs 7, 9, 19, 21, 32, 33, 38, 42, 48, 57, R9-3, 59, 60, 67, 69, 75, and R15 were significantly (≥ 40 -fold) inhibited. This was consistent with our previously published Northern blot analysis of selected RRV latent and lytic mRNAs (12). ORFs 19, 21, 32, 29, 32, 33, 34, 38, 75, and K15 have been classified as tertiary lytic genes in KSHV (25) based upon the temporal order of transcription. A directly comparable genome-wide transcriptional profiling in response to PAA has yet to be published. The drug treatment did not affect primer specificity, as evidenced by identical melting temperatures in the presence and absence of the drug (Fig. 5E). Cluster analysis across three time points (12, 24, and 48 h) verified the individual comparisons (Fig. 5I). At 72 h postinfection, the mRNAs in the PAA-treated cultures accumulated to higher levels compared to untreated cultures because RRV egress

in the untreated cultures destroyed the cells, whereas PAA-treated cultures were arrested prior to viral DNA replication (Fig. 5D). At 96 h, the drug had lost its effect in this high-MOI system (Fig. 5H). This highlights an important limitation of all factors including the onset of viral transcription, mRNA stability, total mRNA level, effects of the drug (PAA), and the overall effect of the virus on cell viability and nucleotide metabolism.

As an alternative approach to classify the temporal order of RRV transcription and to test the sensitivity of our assay, we infected RhFs with RRV at different MOIs including MOIs of 5, 1, 0.1, 0.01, and prepared mRNA at a single time point, 48 h postinfection (Fig. 6A). We hypothesized that our highly sensitive real-time QPCR array would be able to detect transcripts even at the lowest MOI of 0.01. At an MOI of 5, we could detect expression of 66 RRV mRNAs. At an MOI of 1, these mRNAs could be divided into two groups: a highly abundant class (26 mRNAs), which was composed of the RRV immediate-early and early transcripts as identified by time series analysis (Fig. 6A), an intermediate class (five mRNA transcripts), and a less abundant class (35 mRNAs), which included the mRNA transcripts classified as late genes by time series analysis. Importantly, we could detect and cluster RRV mRNAs even if fewer than 1 in 100 cells were infected (MOI of 0.01). Under these conditions, the relative transcription profile of RRV mRNA transcripts was highly correlated ($r = 0.791 \pm 0.167$; $n = 6$) and independent of the MOI. For example, the same group of mRNAs that were highly transcribed at 48 h after RRV infection with an MOI of 0.1 was highly transcribed at 48 h after RRV infections with an MOI of 5. Thus, once RRV enters an RhF cell, lytic gene expression commences in that cell at a fixed pace regardless of whether the neighboring cells are infected or not.

Gene profiling of a 293-RRV-green fluorescent protein latent cell line. We previously reported that RRV can infect HEK293 cells and that the virus establishes a predominantly latent infection in this model (14). This was confirmed by transcriptional array analysis. HEK293 cells were infected with RRV as previously described (14) and subjected to mRNA profiling (Fig. 6B and C). Viral mRNAs were barely detectable, but the relative comparison using the uncentered euclidian metric of rhesus tubulin-normalized data (dCT) showed that most mRNAs were transcribed to various degrees. We did not find strong transcriptional silencing of the entire genome, and just like KSHV-infected HEK293 cells (20) and KSHV-infected BCBL-1s (5), RRV-infected HEK293 cells exhibited some degree of lytic reactivation. In this culture system, TPA can induce complete lytic reactivation and at 48 h after TPA treatment all RRV mRNAs were induced (Fig. 6B). By clustering using a correlation metric on mean-centered data (Fig. 6C), we identified a set of mRNAs that were drastically up-regulated by TPA and that was composed of ORF50/Rta, ORF57/Mta, ORFR8/Zta, and ORFs R9-1, 2, 4, R4, 27, 39, 41, 44, 45, 46, 47, 55, 56, 60, 61, 62, 63, 68, 71, 72, 74, and 26.

Discussion. This study set out to map the temporal order of RRV transcription and to provide a roadmap for future investigations. To achieve this goal, a technology platform was developed that was rapid and quantitative and could be used to measure RRV transcripts even if only 1 in 100 cells was in-

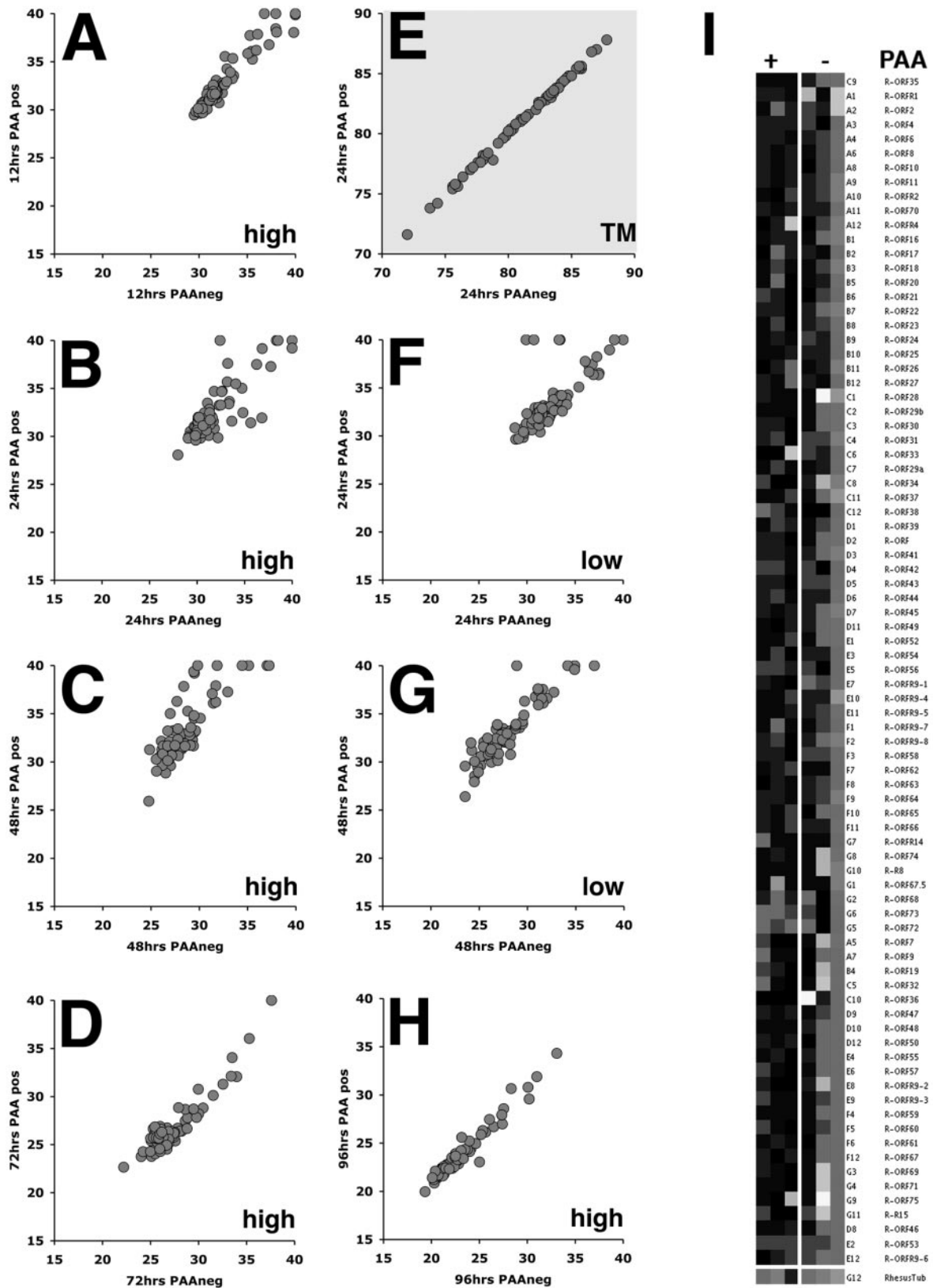


FIG. 5. Impact of cycloheximide and PAA on RRV transcription. RhFs were infected with RRV at an MOI of 1 (panels A to D and H) or an MOI of 0.1 (panels F and G) and either not treated or treated with 50 μ M PAA. Plotted are the CT values for all RRV mRNAs in infected RhFs at 12, 24, 48, 72, and 96 h after infection. Data from RRV-infected, mock-treated cells are on the horizontal axis and data from RRV-infected, PAA-treated cells are plotted on the vertical axis. Panel E plots the melting curves of the reaction products for all RRV primers at 24 h after infection for RRV-infected, PAA-treated (vertical) and RRV-infected, untreated cells. Panel I shows standard correlation-based, hierarchical clustering of time points 12, 24, and 48 h in the presence or absence of PAA. Black indicates low and gray/white high relative levels of the corresponding viral mRNAs. pos, positive; neg, negative.

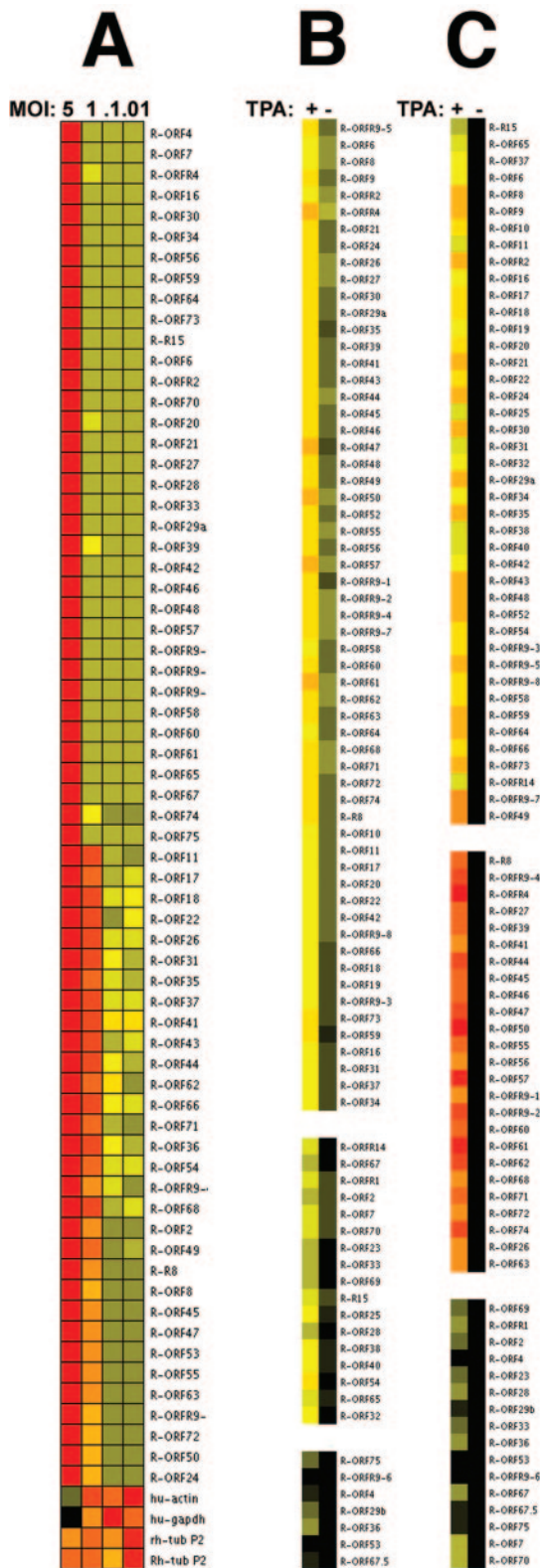


FIG. 6. Applications of the RRV real-time QPCR array. (A) RhFs were infected with RRV at different MOIs (5, 1, 0.1, and 0.01). The real-time QPCR data were normalized to rhesus tubulin (dCT) at 48 h postinfection and are depicted as a heat map. Black indicates low, gray indicates intermediate, and white indicates the highest level of viral mRNA transcripts detected at the different MOIs. (B) Profiles of RRV-infected latent HEK293 cells with and without TPA induction.

ected (Fig. 6A). To date, this represents the only means to quantify viral transcription under conditions of a natural, low-multiplicity infection or in mixtures of permissive and nonpermissive cells. We based the RRV array on real-time QPCR technology because PCR and RT-PCR deliver quantitative information without the need for dilution series, internal competitors, etc. We have recently shown that the SYBR-based method of detection is as sensitive as the TaqMan-based method of detection (37, 38), which reduces the cost of real-time QPCR to the level of traditional PCR without a loss in sensitivity, specificity, or dynamic range. Extensive in silico primer validation eliminated nonspecific signals (Fig. 1 and 2). Comparative array analysis of real-time QPCR data employs the same analytical methods as hybridization-based arrays (16, 19). We previously used this method to analyze KSHV transcription (19) in PEL cells and established a rank order of KSHV transcription after TPA induction, which was largely identical to that obtained in studies that measured mRNA levels by competitive hybridization to spotted viral cDNA arrays (25, 39). A direct comparison of the sensitivity of real-time QPCR arrays to hybridization-based membrane arrays, for which we spotted the real-time QPCR products onto membrane, showed that real-time QPCR-based detection of messages was more sensitive (Vahrson and Dittmer, unpublished). Hence, we were able to measure KSHV transcription in primary 2-by-2-mm punch biopsies, which hitherto was not possible using conventional arrays (16). Hybridization-based arrays profile changes in a nonlinear fashion and tend to overemphasize large changes and compress smaller less-than-twofold variations, whereas real-time QPCR has a linear range of ≥ 6 orders of magnitude (23). This offers an advantage for the analysis of viral mRNAs, which traverse a much larger dynamic range than most cellular transcripts. Cellular microarray measurements are generally verified by real-time QPCR or Northern blot analysis (27). One caveat of microarray-based profiling is of particular concern for studies in herpesvirus transcription: Neither cDNA-based, nor random-primed real-time QPCR-based arrays can distinguish between overlapping transcripts or transcripts that originate on the opposite strand. Using splice site-specific primers, we could distinguish between overlapping, spliced mRNAs in the KSHV LANA, cyclin, vFLIP locus, as well as vIRF-1 and several alpha mRNAs (26). We are currently working on a similar design strategy for known spliced mRNAs in RRV but have noticed that introducing this additional constraint into the design yields greater variation in the PCR efficiency of the individual primer pairs (Vahrson and Dittmer, unpublished). Using strand-specific oligonucleotides as used in the Affymetrix platform, one should be able to distinguish between sense and antisense transcripts, but this approach lacks sensitivity. A similar strategy using strand-specific, gene-specific RRV primers to prime the individual RT reactions can be used to identify antisense mRNAs using PCR-

Cells were treated with TPA or dimethyl sulfoxide for 48 h. Total RNA was isolated and subjected to real-time PCR. The data were normalized to tubulin (dCT). Data are depicted as a heat map using euclidian (B) or standard correlation (C) clustering. Black indicates low, yellow indicates intermediate, and red indicates the highest relative level of viral mRNA transcripts.

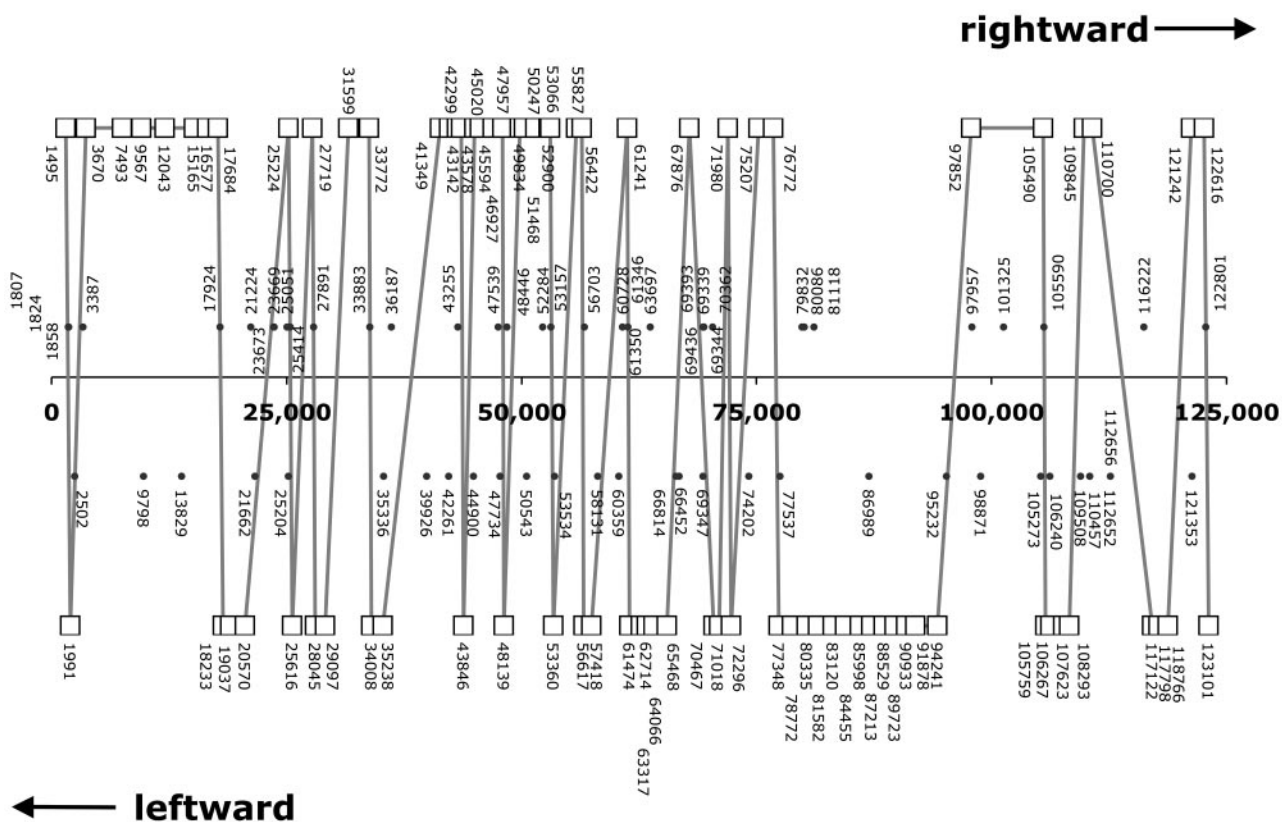


FIG. 7. Locations of RRV primers relative to predicted mRNA termination signals in the RRV genome. Depicted is the location of the forward primer for each RRV ORF (squares) on the RRV genome. Primers for rightward ORFs are indicated as boxes above the horizontal line, and primers for leftward ORFs are indicated below the genome axis. The sequential ORFs (either rightward or leftward) amplified by these primers are connected by vertical lines. The predicted termination signals are indicated with dots.

based arrays. Using the gene-specific reverse primer to specifically reverse transcribe only the sense transcript, we verified that all our primers will detect the mRNA that comprises the coding region for the corresponding protein (data not shown). Based upon the location and orientation of the RRV primers and predicted poly(A) sites (Fig. 7), we can identify regions of co-oriented genes ($n = >3$) for which it is less likely that antisense mRNAs with coding potential exist (e.g., ORFs 4 to 11, 25 to 28, 30 to 33, 34 to 38, 45 to 49, R9.1-8, 58 to 62, 65 to 67, and 71 to 73) and which can be coterminal, such as ORFs 73 to 71 (12). For all other ORFs, a complete transcription map of the RRV genome is required to resolve issues of splicing, antisense, and overlapping transcripts.

The real-time QPCR-based results corroborated our prior Northern blot analysis on a subset of RRV mRNAs (12) and supports the model of a temporal wave of viral gene expression during lytic replication. The majority of mRNAs were induced between 24 and 48 h after infection, while a few mRNAs were not detectable until 96 h postinfection. Overall, there was a good correlation between the transcriptional profiles of RRV de novo infection and KSHV reactivation. One exception to this rule was the latent transcripts for ORF71/vFLIP, 72/vCyc, and 73/LANA, which were dramatically induced upon RRV de novo infection. By contrast, LANA mRNA levels do not significantly increase after KSHV reactivation of PELs (19) and in fact appear to decrease after infection of semipermissive

cells (28). The role for ORF73/LANA in RRV (14), HVS (3, 8, 55), and KSHV (2, 9, 10, 21, 22, 24) is similar for all three viruses, since LANA ensures the maintenance of the viral episome by physically tethering viral DNA to cellular chromosomes through its interaction with cellular factors (29). In addition, LANA has been shown to inhibit lytic viral replication and reactivation in HVS, RRV, and KSHV (14, 31, 49).

RRV transcription profiling during de novo infection of RhFs revealed that the temporal order of viral transcription was conserved among the gamma herpesviruses and supports the hypothesis that RRV Rta/ORF50, the master regulator of lytic transcription (33, 52), is one of the first genes to be expressed. Rta/ORF50 is highly conserved in sequence and function among the rhadinoviruses (11). Once Rta/ORF50 is expressed, viral transcription proceeds in a fixed pattern until complete lytic replication is achieved. RRV transcription in an infected cell is independent of the RRV status of the neighboring cells (Fig. 5). Interestingly, the expression of the mRNAs for the R9-1 through R9-5 genes, which represent the RRV viral interferon (vIRF) genes, was not coregulated since the mRNAs for R9-4 and R9-5 were induced early, while the other R9 mRNAs were induced late. This suggests that the multiply duplicated vIRF genes are expressed at different times in the viral life cycle and parallel the situation of the multiple KSHV vIRFs, which are differentially expressed at different phases of the viral life cycle (7, 16, 35). In conclusion,

we have developed a high-throughput RRV QPCR array that is capable of profiling gene transcription from the entire RRV genome simultaneously. An added benefit of this system is the sensitivity of this QPCR array, which will allow us to determine the RRV transcription profile *in vivo*, in the experimentally infected rhesus macaque.

We thank all the members of the Damania and Dittmer labs for helpful suggestions and Chelsey Hilsher for technical support.

This work was supported by NIH grant CA109232 to D.P.D. and grants from the American Association for Cancer Research (AACR) and the American Heart Association (0355852U) and NIH grants CA096500 and AI58093 to B.D. C. M. Gonzalez is supported by NIH grant CA096500-S, and S. M. DeWire is supported, in part, by an American Heart Association predoctoral fellowship (0315389U).

REFERENCES

- Alexander, L., L. Denenkamp, A. Knapp, M. Auerbach, S. Czajak, B. Damania, and R. C. Desrosiers. 2000. The primary sequence of rhesus rhadinovirus isolate 26-95: sequence similarities to Kaposi's sarcoma herpesvirus and rhesus rhadinovirus isolate 17577. *J. Virol.* **74**:3388-3398.
- Ballestas, M. E., P. A. Chatis, and K. M. Kaye. 1999. Efficient persistence of extrachromosomal KSHV DNA mediated by latency-associated nuclear antigen. *Science* **284**:641-644.
- Calderwood, M. A., K. T. Hall, D. A. Matthews, and A. Whitehouse. 2004. The herpesvirus saimiri ORF73 gene product interacts with host-cell mitotic chromosomes and self-associates via its C terminus. *J. Gen. Virol.* **85**:147-153.
- Cesarman, E., Y. Chang, P. S. Moore, J. W. Said, and D. M. Knowles. 1995. Kaposi's sarcoma-associated herpesvirus-like DNA sequences in AIDS-related body-cavity-based lymphomas. *N. Engl. J. Med.* **332**:1186-1191.
- Chan, S. R., C. Bloomer, and B. Chandran. 1998. Identification and characterization of human herpesvirus-8 lytic cycle-associated ORF 59 protein and the encoding cDNA by monoclonal antibody. *Virology* **240**:118-126.
- Chang, Y., E. Cesarman, M. S. Pessin, F. Lee, J. Culpepper, D. M. Knowles, and P. S. Moore. 1994. Identification of herpesvirus-like DNA sequences in AIDS-associated Kaposi's sarcoma. *Science* **266**:1865-1869.
- Chen, J., K. Ueda, S. Sakakibara, T. Okuno, and K. Yamanishi. 2000. Transcriptional regulation of the Kaposi's sarcoma-associated herpesvirus viral interferon regulatory factor gene. *J. Virol.* **74**:8623-8634.
- Collins, C. M., M. M. Medveczky, T. Lund, and P. G. Medveczky. 2002. The terminal repeats and latency-associated nuclear antigen of herpesvirus saimiri are essential for episomal persistence of the viral genome. *J. Gen. Virol.* **83**:2269-2278.
- Cotter, M. A., II, and E. S. Robertson. 1999. The latency-associated nuclear antigen tethers the Kaposi's sarcoma-associated herpesvirus genome to host chromosomes in body cavity-based lymphoma cells. *Virology* **264**:254-264.
- Cotter, M. A., II, C. Subramanian, and E. S. Robertson. 2001. The Kaposi's sarcoma-associated herpesvirus latency-associated nuclear antigen binds to specific sequences at the left end of the viral genome through its carboxy-terminus. *Virology* **291**:241-259.
- Damania, B. J. J., B. S. Bowser, S. M. DeWire, M. Staudt, and D. P. Dittmer. Unpublished data.
- DeWire, S. M., M. A. McVoy, and B. Damania. 2002. Kinetics of expression of rhesus monkey rhadinovirus (RRV) and identification and characterization of a polycistronic transcript encoding the RRV Orf50/Rta, RRV R8, and R8.1 genes. *J. Virol.* **76**:9819-9831.
- DeWire, S. M., E. S. Money, S. P. Krall, and B. Damania. 2003. Rhesus monkey rhadinovirus (RRV): construction of a RRV-GFP recombinant virus and development of assays to assess viral replication. *Virology* **312**:122-134.
- DeWire, S. M., and B. Damania. 2005. The latency-associated nuclear antigen of rhesus monkey rhadinovirus inhibits viral replication through repression of Orf50/Rta transcriptional activation. *J. Virol.* **79**:3127-3138.
- Dezube, B. J., M. Zambela, D. R. Sage, J. F. Wang, and J. D. Fingerhuth. 2002. Characterization of Kaposi sarcoma-associated herpesvirus/human herpesvirus-8 infection of human vascular endothelial cells: early events. *Blood* **100**:888-896.
- Dittmer, D. P. 2003. Transcription profile of Kaposi's sarcoma-associated herpesvirus in primary Kaposi's sarcoma lesions as determined by real-time PCR arrays. *Cancer Res.* **63**:2010-2015.
- Dittmer, D. P., W. Vahrson, M. R. Staudt, J. F. Papin, R. Hines-Boykin, and F. D. Fakhari. 2004. Real-time quantitative PCR arrays for virally associated cancers. *Cancer Genomics Proteomics* **1**:117-124.
- Eisen, M. B., P. T. Spellman, P. O. Brown, and D. Botstein. 1998. Cluster analysis and display of genome-wide expression patterns. *Proc. Natl. Acad. Sci. USA* **95**:14863-14868.
- Fakhari, F., and D. Dittmer. 2002. Charting latency transcripts in Kaposi's sarcoma-associated herpesvirus by whole-genome real-time quantitative reverse transcription-PCR. *J. Virol.* **76**:6213-6223.
- Foreman, K. E., J. Friborg, W. P. Kong, C. Woffendin, P. J. Polverini, B. J. Nickoloff, and G. J. Nabel. 1997. Propagation of a human herpesvirus from AIDS-associated Kaposi's sarcoma. *N. Engl. J. Med.* **336**:163-171.
- Garber, A. C., M. A. Shu, J. Hu, and R. Renne. 2001. DNA binding and modulation of gene expression by the latency-associated nuclear antigen of Kaposi's sarcoma-associated herpesvirus. *J. Virol.* **75**:7882-7892.
- Grundhoff, A., and D. Ganem. 2003. The latency-associated nuclear antigen of Kaposi's sarcoma-associated herpesvirus permits replication of terminal repeat-containing plasmids. *J. Virol.* **77**:2779-2783.
- Heid, C. A., J. Stevens, K. J. Livak, and P. M. Williams. 1996. Real time quantitative PCR. *Genome Res.* **6**:986-994.
- Hu, J., A. C. Garber, and R. Renne. 2002. The latency-associated nuclear antigen of Kaposi's sarcoma-associated herpesvirus supports latent DNA replication in dividing cells. *J. Virol.* **76**:11677-11687.
- Jenner, R. G., M. M. Alba, C. Boshoff, and P. Kellam. 2001. Kaposi's sarcoma-associated herpesvirus latent and lytic gene expression as revealed by DNA arrays. *J. Virol.* **75**:891-902.
- Jeong, J., J. Papin, and D. Dittmer. 2001. Differential regulation of the overlapping Kaposi's sarcoma-associated herpesvirus vGCR (orf74) and LANA (orf73) promoters. *J. Virol.* **75**:1798-1807.
- Klein, U., A. Gloghini, G. Gaidano, A. Chadburn, E. Cesarman, R. Dalla-Favera, and A. Carbone. 2003. Gene expression profile analysis of AIDS-related primary effusion lymphoma (PEL) suggests a plasmablastic derivation and identifies PEL-specific transcripts. *Blood* **101**:4115-4121.
- Krishnan, H. H., P. P. Naranatt, M. S. Smith, L. Zeng, C. Bloomer, and B. Chandran. 2004. Concurrent expression of latent and a limited number of lytic genes with immune modulation and antiapoptotic function by Kaposi's sarcoma-associated herpesvirus early during infection of primary endothelial and fibroblast cells and subsequent decline of lytic gene expression. *J. Virol.* **78**:3601-3620.
- Krithivas, A., M. Fujimuro, M. Weidner, D. B. Young, and S. D. Hayward. 2002. Protein interactions targeting the latency-associated nuclear antigen of Kaposi's sarcoma-associated herpesvirus to cell chromosomes. *J. Virol.* **76**:11596-11604.
- Lagunoff, M., J. Bechtel, E. Venetsanos, A. M. Roy, N. Abbey, B. Herndier, M. McMahon, and D. Ganem. 2002. De novo infection and serial transmission of Kaposi's sarcoma-associated herpesvirus in cultured endothelial cells. *J. Virol.* **76**:2440-2448.
- Lan, H. C., M. A. Chambers, J. A. Ferguson, K. K. Srivastava, and P. G. Reddy. 1996. Effect of bovine herpesvirus-1 on expression of interleukin-2 receptors and effect of interleukin-12 on lymphocyte proliferation. *Vet. Microbiol.* **49**:59-66.
- Lossos, I. S., D. K. Czerwinski, M. A. Wechsler, and R. Levy. 2003. Optimization of quantitative real-time RT-PCR parameters for the study of lymphoid malignancies. *Leukemia* **17**:789-795.
- Lukac, D. M., R. Renne, J. R. Kirshner, and D. Ganem. 1998. Reactivation of Kaposi's sarcoma-associated herpesvirus infection from latency by expression of the ORF 50 transactivator, a homolog of the EBV R protein. *Virology* **252**:304-312.
- Mansfield, K., S. V. Westmoreland, C. D. DeBakker, S. Czajak, A. A. Lackner, and R. C. Desrosiers. 1999. Experimental infection of rhesus and pig-tailed macaques with macaque rhadinoviruses. *J. Virol.* **73**:10320-10328.
- Moore, P. S., and Y. Chang. 2003. Kaposi's sarcoma-associated herpesvirus immunoevasion and tumorigenesis: two sides of the same coin? *Annu. Rev. Microbiol.* **57**:609-639.
- Nakamura, H., M. Lu, Y. Gwack, J. Souvlis, S. L. Zeichner, and J. U. Jung. 2003. Global changes in Kaposi's sarcoma-associated virus gene expression patterns following expression of a tetracycline-inducible Rta transactivator. *J. Virol.* **77**:4205-4220.
- Papin, J., W. Vahrson, R. Hines-Boykin, D. P. Dittmer. 2004. Real-time quantitative PCR analysis of viral transcription. Quantifying total viral gene transcription, p. 449-480. *In* P. Lieberman (ed.), *Methods in molecular virology (DNA viruses)*. Humana Press, Totowa, N.J.
- Papin, J. F., W. Vahrson, and D. P. Dittmer. 2004. SYBR green-based real-time quantitative PCR assay for detection of West Nile virus circumvents false-negative results due to strain variability. *J. Clin. Microbiol.* **42**:1511-1518.
- Paulose-Murphy, M., N. K. Ha, C. Xiang, Y. Chen, L. Gillim, R. Yarchoan, P. Meltzer, M. Bittner, J. Trent, and S. Zeichner. 2001. Transcription program of human herpesvirus 8 (Kaposi's sarcoma-associated herpesvirus). *J. Virol.* **75**:4843-4853.
- Pfaffl, M. W. 2001. A new mathematical model for relative quantification in real-time RT-PCR. *Nucleic Acids Res.* **29**:e45. [Online.]
- Pfaffl, M. W., G. D. W. Horgan, and L. Dempfle. 2002. Relative expression software tool (REST) for group-wise comparison and statistical analysis of relative expression results in real-time PCR. *Nucleic Acids Res.* **30**:e36. [Online.]
- Renne, R., D. Blackburn, D. Whitby, J. Levy, and D. Ganem. 1998. Limited transmission of Kaposi's sarcoma-associated herpesvirus in cultured cells. *J. Virol.* **72**:5182-5188.

43. **Renne, R., W. Zhong, B. Herndier, M. McGrath, N. Abbey, D. Kedes, and D. Ganem.** 1996. Lytic growth of Kaposi's sarcoma-associated herpesvirus (human herpesvirus 8) in culture. *Nat. Med.* **2**:342–346.
44. **Rice, P., I. Longden, and A. Bleasby.** 2000. EMBOSS: the European Molecular Biology Open Software Suite. *Trends Genet.* **16**:276–277.
45. **Rochford, R., M. L. Lutzke, R. S. Alfinito, A. Clavo, and R. D. Cardin.** 2001. Kinetics of murine gammaherpesvirus 68 gene expression following infection of murine cells in culture and in mice. *J. Virol.* **75**:4955–4963.
46. **Rozen, S., and H. J. Skaletsky.** 1998. Primer3 software distribution. http://frodo.wi.mit.edu/primer3/primer3_code.html.
47. **Sakurada, S., H. Katano, T. Sata, H. Ohkuni, T. Watanabe, and S. Mori.** 2001. Effective human herpesvirus 8 infection of human umbilical vein endothelial cells by cell-mediated transmission. *J. Virol.* **75**:7717–7722.
48. **Sarid, R., O. Flore, R. A. Bohenzky, Y. Chang, and P. S. Moore.** 1998. Transcription mapping of the Kaposi's sarcoma-associated herpesvirus (human herpesvirus 8) genome in a body cavity-based lymphoma cell line (BC-1). *J. Virol.* **72**:1005–1012.
49. **Schafer, A., D. Lengenfelder, C. Grillhosi, C. Wieser, B. Fleckenstein, and A. Ensser.** 2003. The latency-associated nuclear antigen homolog of herpesvirus saimiri inhibits lytic virus replication. *J. Virol.* **77**:5911–5925.
50. **Searles, R. P., E. P. Bergquam, M. K. Axthelm, and S. W. Wong.** 1999. Sequence and genomic analysis of a rhesus macaque rhadinovirus with similarity to Kaposi's sarcoma-associated herpesvirus/human herpesvirus 8. *J. Virol.* **73**:3040–3053.
51. **Soulier, J., L. Grollet, E. Oksenhendler, P. Cacoub, D. Cazals-Hatem, P. Babinet, M. F. d'Agay, J. P. Clauvel, M. Raphael, L. Degos, et al.** 1995. Kaposi's sarcoma-associated herpesvirus-like DNA sequences in multicentric Castelman's disease. *Blood* **86**:1276–1280.
52. **Sun, R., S. F. Lin, L. Gradoville, Y. Yuan, F. Zhu, and G. Miller.** 1998. A viral gene that activates lytic cycle expression of Kaposi's sarcoma-associated herpesvirus. *Proc. Natl. Acad. Sci. USA* **95**:10866–10871.
53. **Swanstrom, R. I., K. Pivo, and E. K. Wagner.** 1975. Restricted transcription of the herpes simplex virus genome occurring early after infection and in the presence of metabolic inhibitors. *Virology* **66**:140–150.
54. **Vandesompele, J., K. De Preter, F. Pattyn, B. Poppe, N. Van Roy, A. De Paepe, and F. Speleman.** 2002. Accurate normalization of real-time quantitative RT-PCR data by geometric averaging of multiple internal control genes. *Genome Biol.* **3**:RESEARCH0034. [Online.]
55. **Verma, S. C., and E. S. Robertson.** 2003. ORF73 of herpesvirus Saimiri strain C488 tethers the viral genome to metaphase chromosomes and binds to *cis*-acting DNA sequences in the terminal repeats. *J. Virol.* **77**:12494–12506.
56. **Wang, Y., O. T. Chong, and Y. Yuan.** 2004. Differential regulation of K8 gene expression in immediate-early and delayed-early stages of Kaposi's sarcoma-associated herpesvirus. *Virology* **325**:149–163.
57. **Wong, S. W., E. P. Bergquam, R. M. Swanson, F. W. Lee, S. M. Shiigi, N. A. Avery, J. W. Fanton, and M. K. Axthelm.** 1999. Induction of B cell hyperplasia in simian immunodeficiency virus-infected rhesus macaques with the simian homologue of Kaposi's sarcoma-associated herpesvirus. *J. Exp. Med.* **190**:827–840.
58. **Yuan, Y.** 2004. Identification and characterization of herpesviral immediate-early genes, p. 231–244. *In* P. Lieberman (ed.), *Methods in molecular virology (DNA viruses)*. Humana Press, Totowa, N.J.
59. **Zhong, W., H. Wang, B. Herndier, and D. Ganem.** 1996. Restricted expression of Kaposi sarcoma-associated herpesvirus (human herpesvirus 8) genes in Kaposi sarcoma. *Proc. Natl. Acad. Sci. USA* **93**:6641–6646.
60. **Zhu, F. X., T. Cusano, and Y. Yuan.** 1999. Identification of the immediate-early transcripts of Kaposi's sarcoma-associated herpesvirus. *J. Virol.* **73**:5556–5567.
61. **Zoetewij, J. P., S. T. Eyes, J. M. Orenstein, T. Kawamura, L. Wu, B. Chandran, B. Forghani, and A. Blauvelt.** 1999. Identification and rapid quantification of early- and late-lytic human herpesvirus 8 infection in single cells by flow cytometric analysis: characterization of antiherpesvirus agents. *J. Virol.* **73**:5894–5902.